Available online at www.sciencedirect.com
ScienceDirect
Fusion Engineering and Design 82 (2007) 1153–1160
Fusion Engineering and Design
www.elsevier.com/locate/fusengdes

# Towards model-based current profile control at DIII-D

Y. Ou [a], T.C. Luce [b], E. Schuster [a,*], J.R. Ferron [b], M.L. Walker [b], C. Xu [a], D.A. Humphreys [b]

[a] *Department of Mechanical Engineering and Mechanics, Lehigh University, Bethlehem, PA, USA*
[b] *General Atomics, San Diego, CA, USA*

Received 25 September 2006; received in revised form 9 April 2007; accepted 10 April 2007
Available online 12 June 2007

**Abstract**

A key goal in control of an advanced tokamak (AT) discharge is to maintain safety factor ($q$) and pressure profiles that are compatible with both MHD stability at high toroidal beta and a high fraction of the self-generated bootstrap current. This will enable high fusion gain and non-inductive sustainment of the plasma current for steady-state operation. In this work we report progress towards enabling model-based active control of the current profile at DIII-D. Initial results on modeling-for-control and simulation of the dynamic evolution of the poloidal flux profile during and just following the ramp-up of the plasma current are presented. The magnetic diffusion equation is combined with empirical correlations obtained at DIII-D for the density, temperature and non-inductive current to introduce a simplified dynamic model describing the evolution of the poloidal flux, and therefore the $q$ profile, during the inductive phase of the discharge. The physical model is rewritten in a control-oriented formulation and the control challenges asocciated with the problem are discussed.


*Keywords:* Current profile control; Modeling-for-control

## 1. Introduction

Advanced tokamak (AT) operation scenarios [1] are characterized by a high confinement state with improved MHD stability, which yields a strong improvement of the plasma performance quantified by the increase of the energy confinement time and plasma pressure. In such conditions a dominant fraction of the plasma current is self-generated by the neoclassical bootstrap mechanism, which reduces the requirement on externally driven non-inductive current for steady-state operation. Setting up a suitable current profile, characterized by a weakly reversed magnetic shear, has been demonstrated to be a key condition for one possible advanced scenario with improved confinement and possible steady-state operation [2].

Although this research area is in its infancy, recent experiments at different devices around the world (JET [3,4], DIII-D, JT-60U [5], Tore Supra [6]) have demon-

* Corresponding author.
*E-mail address:* schuster@lehigh.edu (E. Schuster).

0920-3796/$ – see front matter © 2007 Elsevier B.V. All rights reserved.
doi:10.1016/j.fusengdes.2007.04.016

strated significant progress in achieving profile control. At JET, different current and temperature equilibrium target profiles have been reached and sustained for several seconds during the flat-top current phase. The control scheme relies on the experimental identification of a linearized static response model, using lower hybrid current drive (LHCD), ion cyclotron resonance heating (ICRH) and neutral beam injection (NBI) as actuators. The controller, which finally reduces to a PID incorporating information of the static response of the system, has been shown effective when rapid plasmas events are absent.

In contrast to the JET approach, experiments at DIII-D focus on creating the desired $q$ profile during the plasma current ramp-up and early flat-top phases with the aim of maintaining this target profile during the subsequent phases of the discharge. Active feedback control of the evolution of $q(0)$ and $q_{\min}$ during the initial phase of the discharge has been already demonstrated at DIII-D [7] changing the plasma conductivity through electron heating, and therefore modifying the rate of relaxation of the current profile. The $q$ profile is obtained in real time from a complete equilibrium reconstruction using data from the MSE diagnostic. The controller requests a power level to the actuator (electron cyclotron heating (ECH) or neutral beam heating (NBH)) which is equal to preprogrammed feedforward value plus the error in $q$ times a proportional gain (P controller). Present limitations of this controller (oscillations and instability) motivate the design of a model-based controller that takes into account the dynamics of the $q$ response to the actuators. This paper reports progress at DIII-D in this direction.

A substantial experimental physics effort has been going on for several years to develop predictive models for evolution of poloidal flux, or equivalently, current profiles in toroidal plasmas. Our work draws on the result of those efforts but does not supersede it, since our purpose is simply the conversion of this accepted physics model to a form useful for control. We focus on introducing the model and discussing its qualitative behavior. It is important to note that we are modeling-for-control and not for physical understanding and, consequently, the model needs only to capture the dominant effects of the system dynamics because one of the main characteristics of feedback is the ability to deal with model uncertainties. It is often not possible, however, to assess the true requirements for model accuracy until experimental tests of the controller are performed.

This paper is organized as follows. In Section 2, a dynamic model for the poloidal flux $\psi_{\rm p}$ is introduced. Section 3 describes the control objectives during the different phases of the discharge. Models for the density, temperature, parallel current, and resistivity during the inductive phase of the discharge, as well as a control-oriented dynamic model for the poloidal flux evolution, are introduced in Section 4. Simulation results are presented in Section 5. Section 6 discusses the control needs for the inductive phase of the discharge. Finally, conclusions and identified future work are presented in Section 7.

## 2. Current profile evolution

From the conservation of the magnetic field $\bar{B}$, $\nabla \cdot \bar{B} = 0$, we can write it as the curl of a vector potential, i.e., $\bar{B} = \nabla \times \bar{A}$. In cylindrical coordinates $\bar{R} = (R, \phi, Z)$, we write the vector potential as $\bar{A} = (A_R, A_\phi, A_Z)$. Assuming an axisymmetric configuration, i.e., $\partial/\partial\phi = 0$, the magnetic field results

$$\bar{B} = \left( -\frac{1}{R}\frac{\partial \psi}{\partial Z}, \frac{f}{R}, \frac{1}{R}\frac{\partial \psi}{\partial R} \right), \tag{1}$$

where we define the stream function $\psi(R, Z) = RA_\phi(R, Z)$, closely related to the poloidal flux $\psi_{\rm p}$,

$$\psi_{\rm p} = \int \bar{B}_{\rm p} \cdot {\rm d}\bar{S} = \int_0^{2\pi} {\rm d}\phi \int_0^R RB_Z(R, Z)\,{\rm d}R = 2\pi\psi \tag{2}$$

as the poloidal flux per radian inside a major radius $R$, and $f(R, Z) = RB_\phi(R, Z)$. The magnetic surface $\psi(\bar{R})$=constant, is such that all magnetic lines of force lie upon on that surface, i.e., $\nabla\psi(\bar{R}) \cdot \bar{B} = 0$.

From Ampere's law, $\nabla \times \bar{B} = \mu_{\rm o}\bar{\jmath}$, where $\bar{\jmath}$ is the current density and $\mu_{\rm o}$ is the vacuum magnetic permeability, we can write the current density as

$$\bar{\jmath} = \left( -\frac{1}{\mu_{\rm o} R}\frac{\partial f}{\partial Z}, \Delta^*\psi, \frac{1}{\mu_{\rm o} R}\frac{\partial f}{\partial R} \right), \tag{3}$$

$$\begin{aligned} \Delta^*\psi &= -\frac{1}{\mu_{\rm o}}\left[ \frac{\partial}{\partial R}\left( \frac{1}{R}\frac{\partial \psi}{\partial R} \right) + \frac{1}{R}\frac{\partial^2 \psi}{\partial Z^2} \right] \\ &= -\frac{R}{\mu_{\rm o}} \nabla \cdot \left( \frac{\nabla \psi}{R^2} \right) \end{aligned} \tag{4}$$

We are interested in the dynamics of the current density profile, characterized by the resistive time constant $\tau_r = \mu_o a^2/\eta$ ($a$ is the minor radius of the tokamak, $\eta$ is the plasma resistivity), which is the order of a second. On this time scale, we can consider the system to be at equilibrium, i.e., $\nabla p = \bar{j} \times \bar{B}$, where $p$ denotes the plasma pressure. This implies that $\bar{j} \cdot \nabla p = 0$, which in turns implies that $f$ is parallel to $\nabla\psi$, and therefore, a surface quantity too.

We let $\rho$ be an arbitrary coordinate indexing the magnetic surfaces. Any quantity constant on each magnetic surface could be chosen as the variable $\rho$. We choose the mean geometric radius of the magnetic surface as the variable $\rho$, i.e., $\pi B_{\phi,o}\rho^2 = \Phi$, where $\Phi$ is the toroidal flux and $B_{\phi,o}$ is the reference toroidal magnetic field at $R_o$ ($R_o$ can be the geometric center of the plasma $R_{geo}$).

Defining the average of any arbitrary quantity $A$ on a magnetic surface $S$ by $\langle A\rangle = (\partial/\partial V)\int_V A\,\mathrm{d}V$, and considering that $\langle\nabla\cdot A\rangle = (1/V')(\partial(V'\langle A\cdot\nabla\rho\rangle)/\partial\rho)$, where $V' = \partial V/\partial\rho$, we use (1), (3) and (4) to obtain

$$\langle \bar{j}\cdot\bar{B}\rangle = -\frac{f^2}{\mu_o V'}\left\{\frac{\partial}{\partial\rho}\left[\frac{V'}{f}\left\langle\frac{|\nabla\rho|^2}{R^2}\right\rangle\frac{\partial\psi}{\partial\rho}\right]\right\} \tag{5}$$

From Faraday's law, $\nabla\times\bar{E} = -\mathrm{d}\bar{B}/\mathrm{d}t$, where $\bar{E}$ is the electric field, it can be shown that [8,9]

$$\frac{\partial\psi}{\partial t} = -\frac{\langle\bar{E}\cdot\bar{B}\rangle}{\langle R^{-2}\rangle f}. \tag{6}$$

The inductive component of the current density satisfies Ohm's law

$$\bar{E} + \bar{v}\times\bar{B} = \eta(\bar{j} - \bar{j}_{NI}) \tag{7}$$

where $\bar{v}$ is the mean velocity of the particles and $\bar{j}_{NI}$ is the non-inductive current density. Then, combining (5), (6) and (7), it is possible to write

$$\frac{\partial\psi}{\partial t} = \frac{f\eta}{\mu_o\langle R^{-2}\rangle V'}\left\{\frac{\partial}{\partial\rho}\left(\frac{V'}{f}\left\langle\frac{|\nabla\rho|^2}{R^2}\right\rangle\frac{\partial\psi}{\partial\rho}\right)\right\} + \frac{\eta}{f\langle R^{-2}\rangle}\langle\bar{j}_{NI}\cdot\bar{B}\rangle. \tag{8}$$

From the definition of the toroidal flux,

$$\Phi = \int B_\phi\,\mathrm{d}S_\phi = \frac{1}{2\pi}\int\left(\frac{f}{R^2}\right)\mathrm{d}V \tag{9}$$

and $\pi B_{\phi,o}\rho^2 = \Phi$ we can write

$$V' = \frac{\partial V}{\partial\Phi}\frac{\partial\Phi}{\partial\rho} = \frac{4\pi^2\rho B_{\phi,o}}{f\langle R^{-2}\rangle} \tag{10}$$

By defining,

$$F = \frac{R_o B_{\phi,o}}{f},\quad G = \left\langle\frac{R_o^2}{R^2}|\nabla\rho|^2\right\rangle,$$
$$H = \frac{F}{\langle R_o^2/R^2\rangle}, \tag{11}$$

and $\hat{\rho} = \rho/\rho_b$, where $\rho_b$ is the radius of last closed flux surface, and using (10), we can write (8) as

$$\frac{\partial\psi}{\partial t} = \frac{\eta}{\mu_o\rho_b^2\hat{F}^2}\frac{1}{\hat{\rho}}\frac{\partial}{\partial\hat{\rho}}\left(\hat{\rho}\hat{F}\hat{G}\hat{H}\frac{\partial\psi}{\partial\hat{\rho}}\right) + \frac{R_o\hat{H}\eta}{B_{\phi,o}}\langle\bar{j}_{NI}\cdot\bar{B}\rangle \tag{12}$$

where the geometric factors $\hat{F} = F(\hat{\rho})$, $\hat{G} = G(\hat{\rho})$, and $\hat{H} = H(\hat{\rho})$, shown in Fig. 2 (a), have been determined from DIII-D experimental data using the definitions stated above.

The boundary conditions are given by

$$\left.\frac{\partial\psi}{\partial\hat{\rho}}\right|_{\hat{\rho}=0} = 0,\quad \left.\frac{\partial\psi}{\partial\hat{\rho}}\right|_{\hat{\rho}=1} = \frac{\mu_o}{2\pi}\frac{R_o}{\hat{G}|_{\hat{\rho}=1}\hat{H}|_{\hat{\rho}=1}}I(t) \tag{13}$$

where $I(t)$ denotes total plasma current.

The model makes the simplifying assumption that the magnetic geometry is fixed in time. This excludes two potential sources of flux—a change in $\rho_b$ (either by a change in the shape of the last closed flux surface or in $B_{\phi,o}$) and a change in location of the geometric center of the interior flux surfaces relative to that of the last closed flux surface. Changes in $\rho_b$ are small by design in the experiments of interest, but it is straightforward to include this effect in the model for situations where it would be important. Changes in the relative positions of the flux surfaces do occur, but for cases of interest, these happen slowly enough and they can be neglected.

## 3. Control objectives

Fig. 1 shows the different phases of the discharge. During "Phase I" the control goal is to drive the cur-

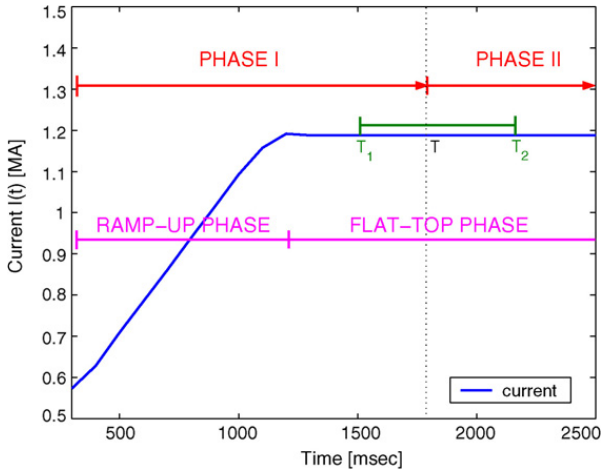


Fig. 1. Current evolution.

rent profile from any arbitrary initial condition to a prescribed target profile at some time $T \in (T_1, T_2)$ in the flat-top phase of the total current $I(t)$ evolution. This prescribed target profile is an equilibrium profile for the current ($\partial(\partial\psi^{\text{target}}/\partial\hat{\rho})/\partial t = 0$) during "Phase II." The available actuators during "Phase I" differ from those used during "Phase II," and are constrained (saturation, rate limit, etc.). Therefore, the prescribed target profile cannot be sustained in equilibrium (steady state) using the available actuators during "Phase I." During "Phase II" the control goal is to regulate the current profile around its equilibrium using as little control effort as possible because the actuators are not only limited in power but also in energy. For this reason, the goal during "Phase I" is to set up an initial profile for "Phase II" as close as possible to its equilibrium profile. During "Phase I," mainly governed by the ramp-up phase, the plasma current is mostly driven by induction. In this case, due to the difference in the time scales, it is possible to neglect the dynamics of the electron temperature and density. Therefore, evolution equations for the electron temperature $T_e(\hat{\rho}, t)$ and density $n(\hat{\rho}, t)$ are not necessary to complete the model. Spatial-temporal laws are used instead (see Section 4, Eqs. (14) and (15)). During "Phase II" (exclusively flat-top phase) the current drive is mainly non-inductive (boostrap current is significant), and for completeness, the magnetic diffusion Eq. (12) must be accompanied by similar parabolic PDEs describing the evolution of the temperature and the density.

## 4. Models for the inductive phase (Phase I)

Simplified models for the density and temperature are chosen for this phase. Based on experimental observations at DIII-D, the profiles are assumed to remain fixed for each specific experiment. The temperature and density responses to the actuators are simply scalar multiples of the reference profiles, which are taken from tokamak discharges associated with the experiment of interest.

### 4.1. Density

The density $n$ is independently controlled, and can be written as

$$n(\hat{\rho}, t) = n^{\text{profile}}(\hat{\rho}) u_n(t), \tag{14}$$

where $n^{\text{profile}}$ is given in Fig. 2 (b). The average density is defined as $\bar{n}(t) = \int_0^1 n(\hat{\rho}, t)\, \mathrm{d}\hat{\rho}$.

### 4.2. Temperature

The temperature $T_e$ is proportional to $(I(t)\sqrt{P_{\text{tot}}(t)})/\bar{n}(t)$, and can be written as

$$T_e(\hat{\rho}, t) = k_{T_e} T_e^{\text{profile}}(\hat{\rho}) \frac{I(t)\sqrt{P_{\text{tot}}(t)}}{\bar{n}(t)} \tag{15}$$

where $T_e^{\text{profile}}$ is given in Fig. 2 (b), $k_{T_e} = 1.7295 \times 10^{10}$, and $P_{\text{tot}}$ is the total power of the non-inductive heating sources (ECH, NBH, etc.).

### 4.3. Parallel current

The non-inductive toroidal current density $\langle \bar{j}_{\text{NI}} \cdot \bar{B} \rangle / B_{\phi,o}$ is written as

$$\frac{\langle \bar{j}_{\text{NI}} \cdot \bar{B} \rangle}{B_{\phi,o}}(\hat{\rho}, t) = C(\hat{\rho}) \frac{P_{\text{tot}}(t)\sqrt{T_e(\hat{\rho}, t)}}{\bar{n}(t)}, \tag{16}$$

where $C(\hat{\rho})$ is a deposition profile. Taking into account (15), we can rewrite (16) as

$$\frac{\langle \bar{j}_{\text{NI}} \cdot \bar{B} \rangle}{B_{\phi,o}} = k_{\text{NIpar}} j_{\text{NIpar}}^{\text{profile}}(\hat{\rho}) \frac{I(t)^{1/2} P_{\text{tot}}(t)^{5/4}}{\bar{n}(t)^{3/2}} \tag{17}$$

where $j_{\text{NIpar}}^{\text{profile}}$ is given in Fig. 2 (b), and $k_{\text{NIpar}} = 1.2139 \times 10^{18}$.

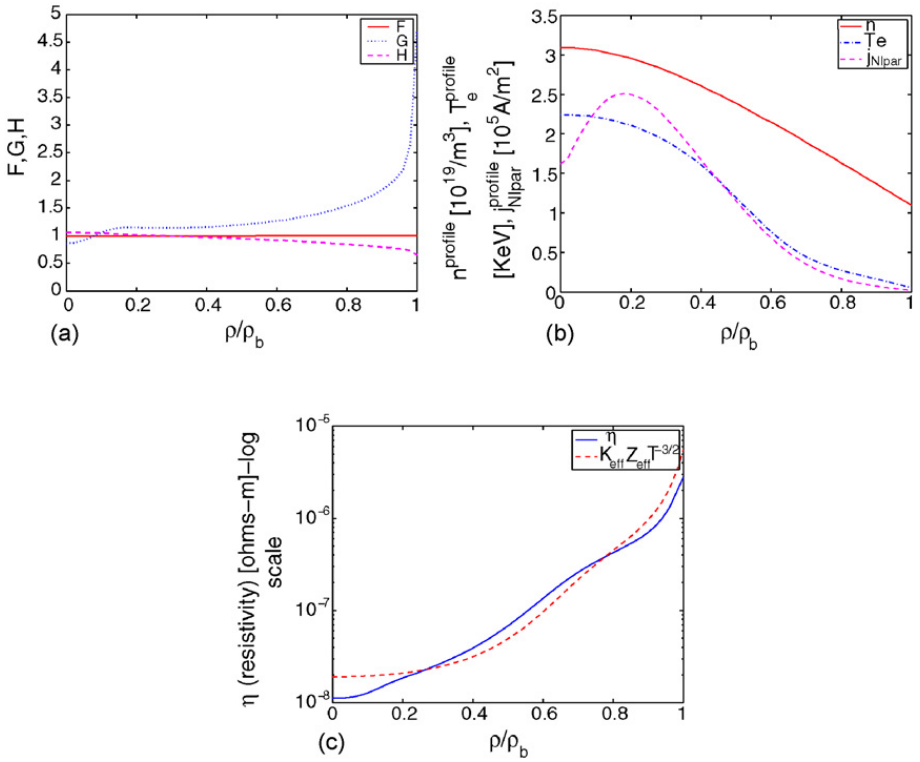


Fig. 2. (a) Geometric factors $\hat{F}$, $\hat{G}$, and $\hat{H}$, (b) density ($n^{\text{profile}}$), temperature ($T_{\text{e}}^{\text{profile}}$), and parallel non-inductive current ($j_{\text{NIpar}}^{\text{profile}}(\hat{\rho})$) profiles, (c) resistivity $\eta$.

### 4.4. Resistivity

The resistivity $\eta$ scales with the temperature $T_{\text{e}}$ as

$$\eta(\hat{\rho}, t) = \frac{k_{\text{eff}} Z_{\text{eff}}}{T_{\text{e}}^{3/2}(\hat{\rho}, t)} \tag{18}$$

Using $Z_{\text{eff}} = 1.5$, it is possible to determine that $k_{\text{eff}} = 4.2702 \times 10^{-8}$. Fig. 2 (c) compares the "computed" $\eta$ using (18) with the measured $\eta$ from the reference DIII-D discharge at the time of the reference profiles.

The poloidal flux diffusion equation is solidly based on Ampere's, Faraday's and Ohm's laws in the usual limit where the Maxwell displacement current is negligible. Experiments in tokamaks have validated the roles of the various terms in this equation. For example, the time scale for electric field penetration was found to be governed by the neoclassical resistivity [10], and the change in the poloidal flux evolution owing to non-inductive current drive has also been verified [11].

We consider now $\bar{n}(t)$, $I(t)$, and $P_{\text{tot}}(t)$ our physical actuators, and put (12) in a control framework.

### 4.5. Diffusivity control

Considering (18), and taking into account (15), we can write

$$\frac{\eta}{\mu_{\text{o}} \rho_{\text{b}}^2 \hat{F}^2}(\hat{\rho}, t) \equiv f_1(\hat{\rho}) u_1(t), \tag{19}$$

$$f_1(\hat{\rho}) = \frac{k_{\text{eff}} Z_{\text{eff}}}{k_{T_{\text{e}}}^{3/2} \mu_{\text{o}} \rho_{\text{b}}^2} \frac{1}{\hat{F}^2(\hat{\rho}) (T_{\text{e}}^{\text{profile}}(\hat{\rho}))^{3/2}}, \tag{20}$$

$$u_1(t) = \left( \frac{\bar{n}(t)}{I(t)\sqrt{P_{\text{tot}}(t)}} \right)^{3/2}. \tag{21}$$

### 4.6. Interior control

Considering (17) and (18) we can write

$$R_{\text{o}} \hat{H} \eta(\hat{\rho}, t) \frac{\langle \bar{\jmath}_{\text{NI}} \cdot \bar{B} \rangle}{B_{\phi,\text{o}}}(\hat{\rho}, t) \equiv f_2(\hat{\rho}) u_2(t), \tag{22}$$

$$f_2(\hat{\rho}) = R_o \hat{H} \mu_o \rho_b^2 \hat{F}^2(\hat{\rho}) k_{\mathrm{NIpar}} j_{\mathrm{NIpar}}^{\mathrm{profile}}(\hat{\rho}) f_1(\hat{\rho}), \quad (23)$$

$$u_2(t) = \frac{\sqrt{P_{\mathrm{tot}}(t)}}{I(t)}. \quad (24)$$

### 4.7. Boundary control

The boundary condition (13) can be written as

$$\left.\frac{\partial \psi}{\partial \hat{\rho}}\right|_{\hat{\rho}=1} \equiv k_3 u_3(t), \quad (25)$$

$$k_3 = \frac{\mu_o}{2\pi} \frac{R_o}{\hat{G}|_{\hat{\rho}=1} \hat{H}|_{\hat{\rho}=1}}, \quad u_3(t) = I(t). \quad (26)$$

### 4.8. Control plant

Considering (19), (22) and (25), we can rewrite the equation for the evolution of the poloidal flux (12) as

$$\frac{\partial \psi}{\partial t} = f_1(\hat{\rho}) u_1(t) \frac{1}{\hat{\rho}} \frac{\partial}{\partial \hat{\rho}} \left( \hat{\rho} f_4(\hat{\rho}) \frac{\partial \psi}{\partial \hat{\rho}} \right) + f_2(\hat{\rho}) u_2(t) \quad (27)$$

with boundary conditions

$$\left.\frac{\partial \psi}{\partial \hat{\rho}}\right|_{\hat{\rho}=0} = 0, \quad \left.\frac{\partial \psi}{\partial \hat{\rho}}\right|_{\hat{\rho}=1} = k_3 u_3(t), \quad (28)$$

and where $f_4(\hat{\rho}) = \hat{F}\hat{G}\hat{H}$. If NBH were considered as the only heating and non-inductive current source, diffusivity and interior control would be coupled through $P_{\mathrm{tot}}$. Use of both NBH and ECH could somewhat, but not completely, decouple them.

As the experiment and the equilibrium change, and therefore the profiles in Fig. 2 (a) and (b), the dependence of $f_1$, $f_2$, and $f_4$ on $\hat{\rho}$ will also change, but the structure of (27) and (28) will remain. Thus, it is important to understand the control challenges associated with this system.

## 5. Simulation results

The system of equations describing the poloidal flux evolution has been successfully implemented in a numerical solver. Fig. 3 shows the profile evolutions for $\iota = 1/q = -(B_{\phi,o}\rho_b^2\hat{\rho})^{-1}(\partial\psi/\partial\hat{\rho})$, $\psi$, and $\langle \bar{\jmath} \cdot \bar{B} \rangle / B_{\phi,o}$, based on the dynamic model (27) and (28),

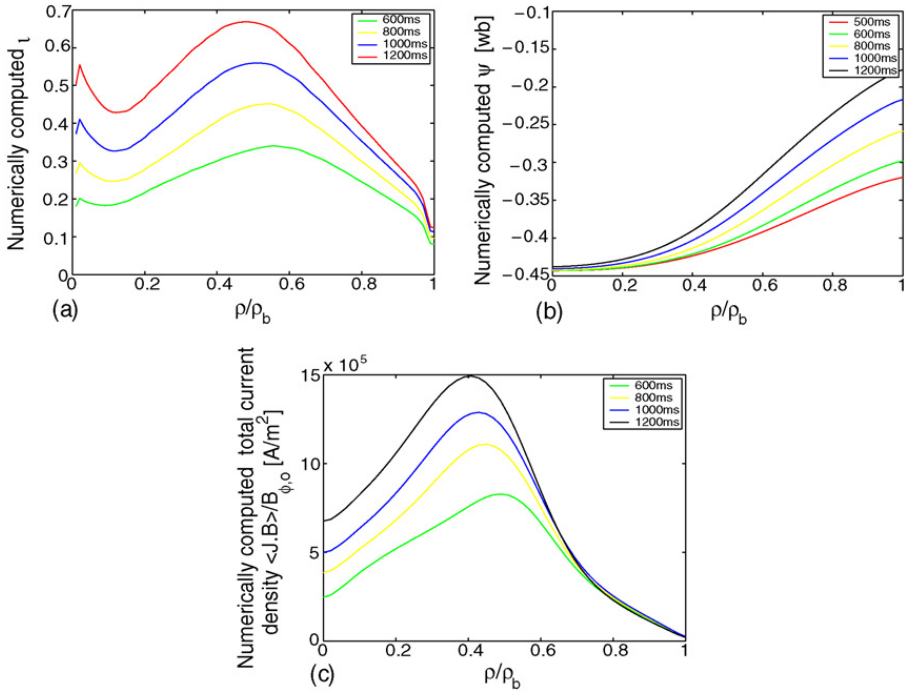


Fig. 3. Simulation of profile evolution: (a) $\iota$, (b) $\psi$, (c) $\langle \bar{\jmath} \cdot \bar{B} \rangle / B_{\phi,o}$.

when $\bar{n}(t)[10^{19}\,\mathrm{m}^{-3}] = 2.7I(t)[\mathrm{MA}]$, $P_{\mathrm{tot}} = 2.6\,\mathrm{MW}$, and the current evolution is that shown in Fig. 1. As expected, the total current density increases with time, consistent with the boundary condition related to the total current at $\hat{\rho} = 1$. The maximum of the current density moves slowly to smaller radius, as expected from a diffusive process. Given the three order of magnitude variation in the plasma resistivity (small in the hot center and large at the cold edge), the current density rapidly equilibrates at the edge, but evolves much more slowly in the center. The small spatial scale structure in $\iota$ at small radius is an artifact of the numerical differencing scheme used to derive this variable from the calculated poloidal flux.

## 6. Control needs

The control of parabolic diffusion-reaction PDE equations such as (27) has been extensively studied using *interior control* (defines a feedback control law for $u_2(t)$), usually making use of model reduction techniques (see Ref. [12] and references therein) or *boundary control* (defines a feedback control law for $u_3(t)$) [13,14]. However, control through $u_1(t)$, what we name *diffusivity control* here, has not been previously considered. In addition, significant actuator constraints must also be considered, which adds to the complexity of the problem.

During "Phase I" an optimal control problem must be solved, where control laws $u_i(t)$, for $i = 1, 2, 3$, are sought to minimize the cost functional

$$J = \frac{1}{2}\int_0^1 \alpha(\hat{\rho})(\iota^*(\hat{\rho}) - \iota(\hat{\rho}, T))^2\,\mathrm{d}\hat{\rho} + \frac{1}{2}\sum_{i=1}^{3}\gamma_i \int_0^T u_i^2(t)\,\mathrm{d}t$$

where $\alpha(\hat{\rho})$ and $\gamma_i$'s are weight functions, and $\iota^*(\hat{\rho})$ is the prescribed target profile. Experimentalists usually describe the target profile in terms of $\iota$ or $q$. In this case, we have chosen to define the cost function in terms of $\iota$, but it can be defined in terms of $q$ as well. This problem has been previously studied for $u_1(t) = \mathrm{cte}$ (cte stands for a constant value); where optimality conditions can be stated using the Maximum Principle and solutions can be obtained using numerical methods [15]. However, due to their high computational demands these optimization techniques based on infinite dimensional models are restricted to open loop control. In addition, this approach must be extended to the $u_1(t) \neq \mathrm{cte}$ case to apply to the current profile control problem in tokamaks.

Model reduction via Inertial Manifold (IM) [16] and Proper Orthogonal Decomposition (POD) [17] have been considered to some extent when $u_1(t) = \mathrm{cte}$ [18,19]. Additional efforts are necessary to be able to address the $u_1(t) \neq \mathrm{cte}$ (nonlinear) case. Once an approximate finite dimensional representation of the system is obtained, many well established control techniques for ordinary differential equations (ODEs) can be considered. In particular, Model Predictive Control (MPC) [20] is well suited to handling constraints within an optimal framework. Although MPC is a control technique widely used for ODE systems, and extensive research has been done in this area, its extension to PDE systems is still an open problem. This is especially true when one takes into account that the eventual approximate, reduced-order, finite dimensional models will be bilinear or driftless (nonlinear), which may not be controllable by continuous control laws [21].

## 7. Conclusions

A simplified, experiment-specific, dynamic model describing the evolution of the poloidal flux, and therefore the $q$ profile, during the inductive phase of the discharge has been introduced. Simulation results show qualitative agreement with experiments. This model will be used for the design of feedback control strategies for the current profile during the ramp-up and early flat-top phases at DIII-D. The proposed model, and the controllers developed based on it, will be tested experimentally. Different control approaches and needs have been discussed.

## Acknowledgments

This work was supported in part by a grant from the Commonwealth of Pennsylvania, Department of Community and Economic Development, through the Pennsylvania Infrastructure Technology Alliance (PITA), the NSF CAREER award program

(ECCS-0645086), and DoE contract number DE-FC02-04ER54698.

## References

[1] T. Taylor, Physics of advanced tokamaks, Plasma Phys. Controlled Fusion 39 (Suppl. 12B) (1997) B47–B73.
[2] M. Murakami, M.R. Wade, C.M. Greenfield, T.C. Luce, J.R. Ferron, H.E. St. John, et al., Progress toward fully noninductive, high beta conditions in DIII-D, Phys. Plasmas 13 (5) (2006) 056106.
[3] D. Moreau, F. Crisanti, X. Litaudon, D. Mazon, P. De Vries, R. Felton, et al., Real-time control of the q-profile in JET for steady state advanced tokamak operation, Nucl. Fusion 43 (9) (2003) 870–882.
[4] L. Laborde, D. Mazon, D. Moreau, A. Murari, R. Felton, L. Zabeo, et al., A model-based technique for integrated real-time profile control in the JET tokamak, Plasma Phys. Controlled Fusion 47 (1) (2005) 155–183.
[5] T. Suzuki, A. Isayama, S. Ide, T. Fujita, T. Oikawa, S. Sakata, et al., Recent RF experiments and application of RF waves to real-time control of safety factor profile in JT-60U, in: AIP Conference, vol. 787, 2005, pp. 279–286.
[6] T. Wijnands, D. Van Houtte, G. Martin, X. Litaudon, P. Froissard, Feedback control of the current profile on Tore Supra, Nucl. Fusion 37 (6) (1997) 777.
[7] J.R. Ferron, P. Gohil, C.M. Greenfield, J. Lohr, T.C. Luce, M.A. Makowski, et al., Feedback control of the safety factor profile evolution during formation of an advanced tokamak discharge, Nucl. Fusion 46 (10) (2006) L13.
[8] J. Blum, Numerical Simulation and Optimal Control in Plasma Physics, Gauthier-Villars Series, Wiley, 1989.
[9] F. Hinton, R. Hazeltine, Theory of plasma transport in toroidal confinement systems, Rev. Modern Phys. 48 (2) (1976) 239–308.
[10] S.H. Batha, F.M. Levinton, A.T. Ramsey, G.L. Schmidt, M.C. Zarnstorff, Local test of parallel electrical resistivity in the Tokamak Fusion Test Reactor, Phys. Plasmas 4 (10) (1997) 3614.
[11] C.B. Forest, K. Kupfer, T.C. Luce, P.A. Politzer, L.L. Lao, M.R. Wade, et al., Determination of the non-inductive current profile in tokamak plasmas, Phys. Rev. Lett. 73 (1994) 2444.
[12] P. Christofides, Nonlinear and Robust Control of PDE Systems, Birkhauser, 2001.
[13] E. Schuster, M. Krstic, Control of a nonlinear PDE system arising from non-burning tokamak plasma transport dynamics, International Journal of Control 76 (11) (2003) 1116–1124.
[14] A. Smyshlyaev, M. Krstic, Closed form boundary state feedbacks for a class of partial integro-differential equations, IEEE Trans. Automatic Control 49 (12) (2004) 2185–2202.
[15] X. Li, J. Yong, Optimal Control Theory for Infinite Dimensional Systems, Birkhauser, 2000.
[16] C. Foias, M. Jolly, I. Kevrekidis, G. Sell, E.S. Titi, On the computation of inertial manifolds, Phys. Lett. A 131 (7–8) (1988) 433–436.
[17] P. Holmes, J. Lumley, G. Berkooz, Turbulence, Coherent Structures, Dynamical Systems and Symmetry, Cambridge University Press, 1996.
[18] M. Bohm, M. Demetriou, S. Reich, I. Rosen, Model reference adaptive control of distributed parameter systems, SIAM J. Control Optimization 36 (1) (1998) 33–81.
[19] K. Kunisch, S. Volkwein, L. Xie, HJB-POD-based feedback design for the optimal control of evolution problems, SIAM J. Appl. Dyn. Syst. 3 (4) (2004) 701–722.
[20] J. Rawlings, Tutorial of model predictive control, IEEE Control Syst. Mag. 20 (3) (2000) 38–52.
[21] R. Brockett, Asymptotic stability and feedback stabilization, in: Differential Geometric Control Theory, Birkhauser, 1983, pp. 181–191.